Direct determination of forces between charged nanogels through coarse-grained simulations

Manuel Quesada-Pérez,[1] José Alberto Maroto-Centeno,[1] Alberto Martín-Molina,[2,3] and Arturo Moncho-Jordá[2,3]
[1]*Departamento de Física, Escuela Politécnica Superior de Linares, Universidad de Jaén, 23700, Linares, Jaén, Spain*
[2]*Departamento de Física Aplicada, Facultad de Ciencias, Universidad de Granada, 18071 Granada, Spain*
[3]*Instituto Carlos I de Física Teórica y Computacional, Facultad de Ciencias, Universidad de Granada, 18071 Granada, Spain*

(Received 6 November 2017; published 19 April 2018)

In this work, electrostatic forces between charged nanogels are explored through coarse-grained simulations. These simulations allow us to explicitly consider the complex topology of these nanoparticles and provide reliable force values to examine highly charged nanogels of a few tens of nanometers. The results obtained here clearly reveal that the electrostatic interactions between these nanoparticles are not governed by the net charge of the nanogel, which includes not only the charge of the polymer network but also the charge of ions inside. Thus two theoretical procedures for predicting effective charges are also proposed and investigated. Both provide predictions of the same order and capture the behavior found for the effective charge obtained from simulations.

DOI: 10.1103/PhysRevE.97.042608

I. INTRODUCTION

Nanogels are nanometer-sized particles that consist of crosslinked polymer networks with the ability to swell in a thermodynamically good solvent. When their mean diameter is of the order of hundreds of nanometers, they are also known as microgels. In any case, the small size of these colloidal particles enables them to develop a rapid kinetic response to environmental stimuli (such as temperature or pH). This stimulus responsiveness makes nanogels excellent candidates for biotechnological applications such as biomaterials and drug delivery [1–3]. Nanogels are also employed as "model atoms" in experiments addressing condensed matter problems such as structure formation, dynamics, or phase transitions [4,5]. Due to the vast assortment of applications, these nanoparticles have gained considerable attention during the last decades.

In many instances, the polymer chains forming nanogels carry ionized groups. Thus the precise knowledge of the electrostatic forces between these nanoparticles is essential in any attempt to understand their behavior and control the processes in which they are involved. However, the theoretical determination of such forces constitutes an issue which has not been fully resolved yet for hard colloids and presents its own peculiarities in soft matter [6,7]. For example, a key feature that distinguishes nanogels from hard colloidal particles is their permeability. Thus electrostatic interactions between nanogels are expected to be governed by the charge of the system formed by the polymeric backbone and the ions inside, to which we will refer to as the net charge of the nanogel.

There are a few theoretical studies supporting this idea [8–10]. In these surveys the complexity of such many-body systems is faced with the help of effective interactions, a powerful tool in statistical mechanics that characterizes the macromolecular aggregates as a whole, including not only the direct interactions between them but also the indirect effects of solvent and small ions. In this way, it is possible to make valuable predictions on the structural and phase behavior of ionic microgels [11–13]. However, it should be mentioned that certain effects, such as the flexibility and fluctuations of the polymer chains or the high degree of crosslinking, are usually neglected by these approaches. In fact, the complex topology of nanogels could justify why theoretical treatments are rarer for these systems. In addition, some approximations made in these treatments might fail for highly charged nanoparticles.

In this work we present coarse-grained simulations of the electrostatic interactions between charged nanogels which allow us to explicitly account for the topology of these polymer networks, the flexibility of their polymer chains, the fluctuations of charge distributions, or the nonexistence of a perfect spherical surface. In the absence of directly measured forces in three dimensions, these results constitute a valuable tool for finding out the precise functional form of this interaction and how these forces depend on the charge of these nanoparticles. In fact, these simulations reveal that the electrostatic forces between nanogels of a few tens of nanometers are not controlled by the bare charge of their backbones or by the net charge. An effective charge must be employed instead. From the results presented here, two theoretical approaches to estimating this parameter are proposed. One of them is an easy and intuitive prescription inspired by the notion of ionic condensation. The other is based on the Ornstein-Zernike (OZ) integral equation theory within the hypernetted-chain closure (HNC).

The rest of the paper is organized as follows. First, the model used and some details on the simulation technique are given. Then the results are presented and discussed. Finally, some outstanding conclusions are highlighted.

II. MODEL AND SIMULATIONS

The coarse-grained picture employed in our simulations is the so-called bead-spring model for polyelectrolyte in which ions and monomer units are represented as spheres whereas the solvent is considered as a dielectric continuum (primitive model). This representation of reality has been widely used in the research of adsorption and collapse of charged polyelectrolytes [14,15] and in the study of different single-nanogel properties [16–23], but here, coarse-grained simulations of two

charged nanogels are employed in the explicit computation of interaction forces between these nanoparticles.

The simulation cell is a cubic box of length L that contains two negatively charged nanogels, monovalent cations, and anions in a fixed number determined by the bulk electrolyte concentration and an excess of monovalent cations neutralizing the charge of the nanogels. Each nanogel particle consists of 100 polyelectrolyte chains connected by 66 crosslinkers. The topology is the same employed in a previous survey [24]. Each polyelectrolyte chain has four monomers to avoid extremely time-consuming simulations. A fraction f of monomers are negatively charged ($f = 0.625, 0.125, 0.25, 0.50, 0.75$, and 1.00) so that the charge of each nanogel is $Ze = -25e$, $-50e, -100e, -200e, -300e$, and $-400e$ (where e is the elementary charge). The diameter of monomers, crosslinkers, and ions is $d = 0.7$ nm. For ions, this size includes the corresponding hydration shell [25]. The short-range repulsion between any pair of these particles due to excluded volume effects was modeled by means of a purely repulsive Weeks-Chandler-Andersen potential:

$$u_{\mathrm{WCA}}(r) = \begin{cases} 4\varepsilon_{\mathrm{LJ}}\left(\frac{d^{12}}{r^{12}} - \frac{d^6}{r^6} + \frac{1}{4}\right) & r \leqslant \sqrt[6]{2}d \\ 0 & r > \sqrt[6]{2}d \end{cases}, \qquad (1)$$

where r is the center-to-center distance between a given pair of particles, $\varepsilon_{\mathrm{LJ}} = 4.11 \times 10^{-21}$ J, and d is the monomer diameter. The interaction connecting monomer units and crosslinkers with their neighbors was modeled by harmonic bonds, $u_{\mathrm{bond}}(r) = 0.5k_{\mathrm{bond}}(r - r_0)^2$, where k_{bond} is the elastic constant (0.4 N/m) and r_0 is the equilibrium length corresponding to this harmonic potential (0.7 nm in this case). All the charged species interact through the Coulomb potential, $u(r) = Z_i Z_j e^2/4\pi\varepsilon_0\varepsilon_r r$, where Z_i is the valence of species i, and ε_0 and ε_r are the vacuum permittivity and relative permittivity of the solvent, respectively.

Initially, both nanogels were placed symmetrically along a diagonal of the cubic simulation cell. The center of the cube coincided with the center of mass (c.m.) of the two nanoparticles (see Fig. 1). The distance between the surface of the nanogels and the nearest side of the cube is 3 times the Debye length (l_D). In this way, the electric double layers of the nanogels are fully developed inside the simulation cell. According to this prescription and the geometry of the initial configuration, the length of the simulation cell is given by $L \approx 2(r/2\sqrt{3} + 3l_D + R_n)$. Three kinds of Monte Carlo (MC) movements were employed: (i) single-particle translations for ions, monomers, and crosslinkers; (ii) translations of the whole nanogels and the ions inside them; and (iii) rotations of the nanogels around their c.m.'s (including also the ions inside). Rotations were attempted with a frequency of 0.002 in all cases. However, the frequency of translations of all the nanogels was 0.05 for the systems ($Z = -100$, 0.1 mM), ($Z = -100$, 0.5 mM), ($Z = -100$, 10 mM), and ($Z = -400$, 1 mM), which have the greatest numbers of particles in the simulation cell, and 0.03 in the other cases. The rest of the movements correspond to single-particle translations. In addition, expansions and contractions of the whole nanogel were employed to accelerate the relaxation of the network during thermalization. In all these movements, maximum displacements were adjusted after periods of 1×10^5 configurations so that its respective acceptance ratio was close to 50%. In the case of single-beads translations, the maximum displacements were individually updated.

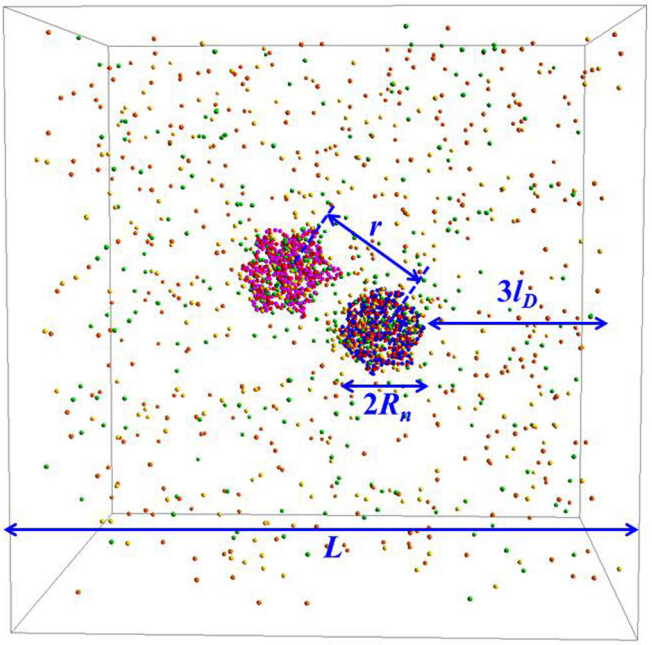

FIG. 1. Snapshot of the simulation cell. L, R_n,l_D, and r denote the length of the simulation box, the mean radius of the nanogels, the Debye length, and the center-to-center distance between the nanogels, respectively. The beads of different colors are neutral and charged monomers of the nanogels and monovalent cations and ions.

Three-direction periodic boundary conditions were applied. Before performing two-nanogel simulations, isolated charged nanogels were simulated following the procedure described in a previous paper to compute their distributions of mass and the ionic profiles [26]. Long-range Coulomb forces were handled through Ewald sums, which were implemented with algorithms and recommendations similar to those reported in previous papers [26,27].

In this work, the mean force between the two nanogels at a given distance was computed from the potential of mean force, which in turn was calculated as follows. First, nanogels were placed at the desired separation. During the runs, the distance between their c.m.'s was allowed to explore a narrow window around the distance under study with the help of a bias potential (an example is briefly commented below) and the probability $P(r)$ of finding their respective c.m.'s at a separation r was computed. For each separation, six independent runs with different initial relative orientations of the nanogels were executed. For thermalization and averaging, 1×10^7 and 4×10^7 MC steps were employed in each run, respectively. Thus a total number of 3×10^8 steps (on average 1.4×10^5 steps per particle) were required to compute the function $P(r)$ in a small interval of r values around the distance under examination. After obtaining $P(r)$, the nanogel-nanogel potential of mean force was computed as $U_{nn}^{pmf}(r) = -k_B T \ln(P(r))$, where k_B is Boltzmann's constant and T is the absolute temperature (298 K). A similar procedure was employed in a previous work for

TABLE I. Radius, net charge, and different effective charges of the nanogels.

$-Z$	Salt concentration (mM)	Radius (nm)	$-Z_{net}$	$-Z_{eff}$ obtained by fitting force	$-Z_{eff}$ estimated from the OZ-HNC formalism	$-Z_{eff}$ estimated from charge-potential profiles
25	1	6.07 ± 0.10	20.9	19.3 ± 0.2	20.5	20.5
50	1	6.24 ± 0.13	36.3	30.3 ± 0.3	33.1	30.4
100	0.1	7.05 ± 0.13	67.0	45.0 ± 0.5	52.2	50.9
100	0.5	6.88 ± 0.12	57.3	38.8 ± 0.2	46.1	41.4
100	1	6.80 ± 0.14	54.2	37.0 ± 0.1	44.0	39.0
100	10	6.61 ± 0.12	40.6	38.8 ± 1.6	38.8	38.2
200	1	7.70 ± 0.14	77.6	42.9 ± 0.2	56.4	48.5
300	1	8.26 ± 0.12	94.7	45.6 ± 0.3	63.4	54.0
400	1	8.65 ± 0.09	109.0	49.8 ± 0.3	71.4	58.1

the computation of potential of mean force of ideal neutral nanogels [24].

III. RESULTS AND DISCUSSION

A. Nanogel properties

Table I summarizes the main properties of the nanogels studied in this work, including the geometrical radius of the nanogel considered in a first approximation as a sphere (R_n), which was computed from the radius of gyration (R_g) considering the relationship between the geometrical radius and radius of gyration of a homogenous sphere, $R_n = \sqrt{5/3}R_g$ [24]. The uncertainties in R_n and R_g were estimated from the fluctuations of R_g^2 in time, which was monitored to check that an equilibrium value was reached after equilibration. The uncertainty in R_n (also included in Table I) is not greater that 2% in the systems studied. Thus nanogel fluctuations seem to be small. However, we should keep in mind that the degree of crosslinking of the nanogels of this work is considerably high.

As mentioned previously, single-nanogel simulations were performed before determining the force between pairs of nanogels. Such simulations provided useful information on charge distribution. In particular, it is possible to compute the charge enclosed by a sphere of radius r centered at the center of mass of the nanogel $Q(r)$ as a function of r, plotted in Fig. 2. As can be seen in such a figure, the absolute value of $Q(r)$ exhibits a maximum at $r \approx R_n$, which can be interpreted as the net charge of the nanogel (Z_{net}) since it included the charge of the polymeric network, the charge inside the nanogel, and the charge in the immediate neighborhood. We might also employ the charge enclosed by R_n, but this yields slightly smaller net charges because part of the nanogel is outside.

$Q(r)$ also presents a small peak in the region $r < R_n$, which reveals that the charge is not uniformly distributed inside the nanogel. This uneven charge distribution might be attributed to the existence of accumulation of charged monomers near the crosslinkers, particularly in the case of highly charged nanogels.

A spherically averaged electric field at a distance r from the center of mass can be obtained from $Q(r)$ applying Gauss' law. Then a spherically averaged electrostatic potential ($\psi(r)$) was estimated integrating this electric field from the border of the simulation cell. The profiles corresponding to this property are plotted in Fig. 3. In general, the behavior of this function is not monotonous inside the nanogel, which is again attributed to uneven charge distributions. This figure also shows that $|e\psi|/k_BT$ is much greater than 1 inside the nanogels studied in this work and even in the proximity of their surfaces for most of them. The normalized electrostatic potential is of the order of 1 (or smaller) in the neighborhood of the particle only in the cases ($Z = -25$,1 mM) and ($Z = -100$,5 mM). This implies that the counterions inside the polymer network as well as the counterions in the vicinity of the nanoparticle are strongly bound to the nanogel (with the two exceptions previously pointed out).

From the data displayed in Figs. 2 and 3 it is possible to construct charge-potential profiles for the nanogels investigated in this work. These profiles are shown in Fig. 4. As mentioned before, the greatest charge of a given profile can be interpreted as the net charge of the nanogel, since it takes place for r values of the order of the nanogel radius.

B. Determining forces and effective charges

The force at a given separation of the centers of mass of the nanogels was determined allowing these nanoparticles to move in an interval of distances $[r_{min}, r_{max}]$ centered in the separation of interest. For instance, to determine the force at 20 nm, the

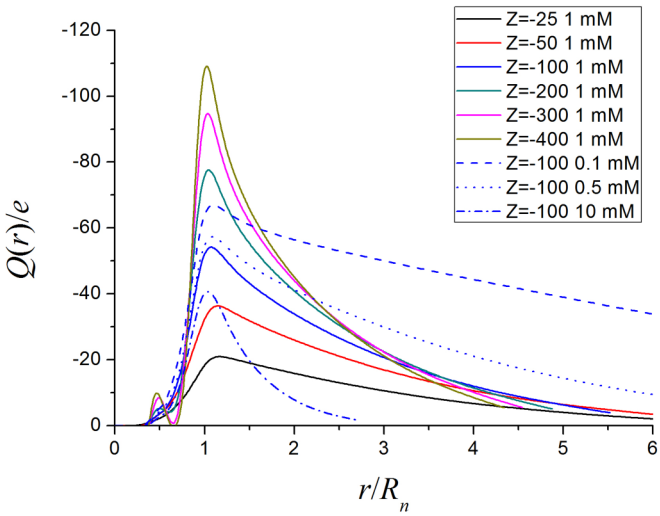

FIG. 2. Charge enclosed by a sphere of radius r (in elementary units), $Q(r)/e$, as a function of the distance to the center of mass (r) normalized by the geometrical radius of the nanogel, R_n.

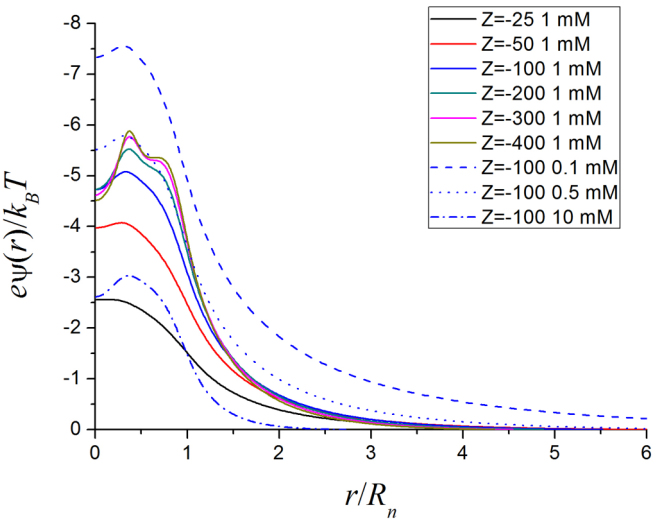

FIG. 3. Normalized electrostatic potential, $e\psi/k_BT$, as a function of the distance to the center of mass (r) normalized by the geometrical radius of the nanogel, R_n.

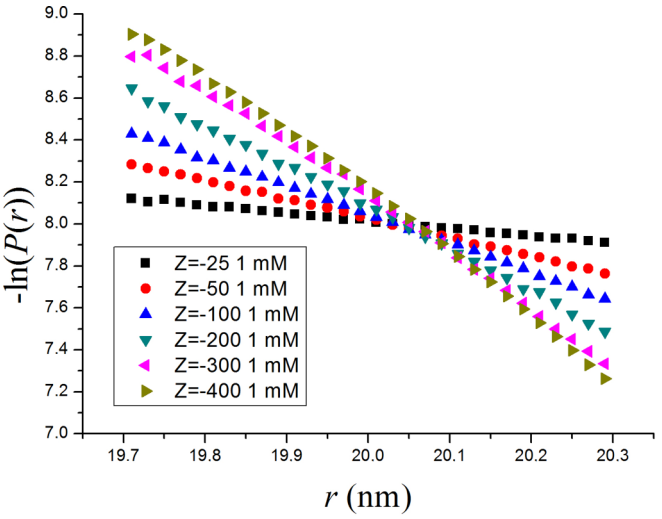

FIG. 5. Minus logarithm of the probability of finding the nanogel c.m.'s at a separation r, $-\ln(P(r))$, as a function of r for different pairs of nanogels at 1 mM (r is restricted to the interval [19.7,20.3] through a bias potential).

movements of the nanogels were restricted to c.m. separations between $r_{\min} = 19.7$ and $r_{\max} = 20.3$ nm. This restriction was implemented through the bias potential

$$u_{\text{bias}}(r) = \begin{cases} 0 & r_{\min} < r < r_{\max} \\ \infty & \text{otherwise} \end{cases}. \qquad (2)$$

Here r is the distance between the c.m.'s of the nanogels. Six independent runs starting from different relative orientations were performed to compute the probability of finding the c.m.'s of the nanogels at a separation r, $P(r)$. Just as an example, Fig. 5 shows $-\ln(P(\text{r}))$ for different pairs of nanogels at 1 mM employed to compute the force when the distance between them is 20 nm. The quantity $-\ln(P(\text{r}))$ can be identified with the normalized nanogel-nanogel potential of mean force, $U_{nn}^{pmf}(r)/k_BT$ (determined except an additive constant). Finally, the mean force was estimated as minus the slope of $U_{nn}^{pmf}(r)$ at the desired distance. It should be also mentioned in relation to this procedure that the mean force can also be determined by fixing the distance between nanogels and averaging the total force between them directly. However, preliminary simulations following this approach revealed that the uncertainty in the contribution due to short-range excluded volume interactions was considerably high. For that reason, the force was derived from the potential in small windows.

Figure 6 shows the forces obtained for each pair of nanogels studied here as a function of the distance between their c.m.'s. It is worth finding out if the functional form of these forces can be derived from the interaction potential proposed by

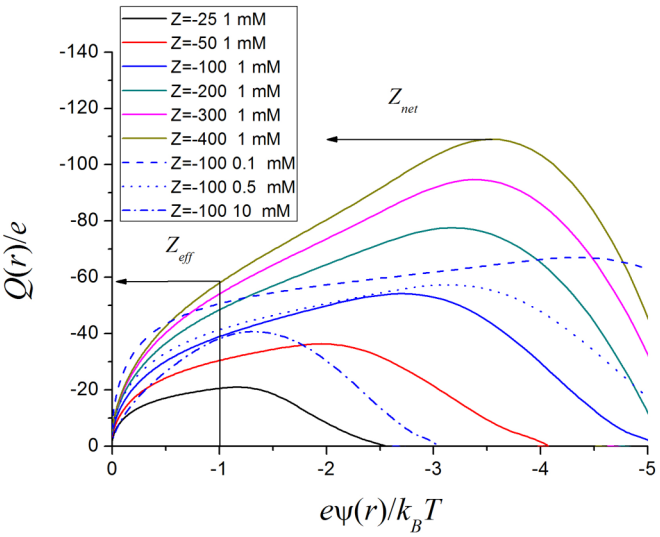

FIG. 4. Charge enclosed by a sphere of radius r (in elementary units), $Q(r)/e$, as a function of normalized electrostatic potential, $e\psi/k_BT$.

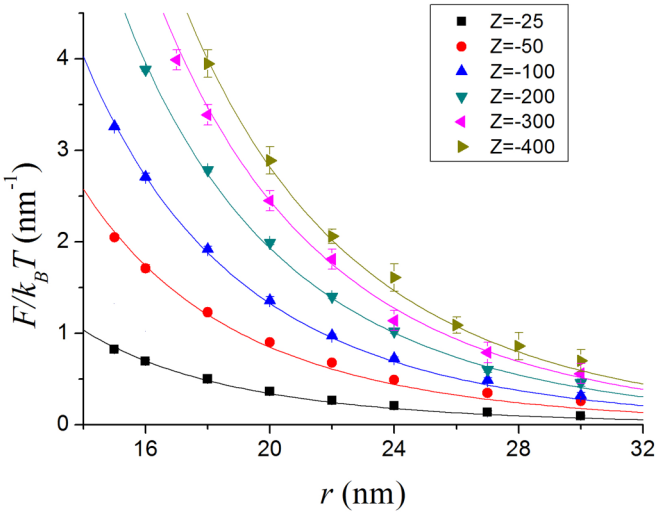

FIG. 6. Force (F) between a pair of nanogels as a function of the distance (r) between their c.m.'s obtained in simulations for the nanogels studied at 1 mM. Lines denote the fits obtained using Denton's potential and the charge as the only adjustable parameter.

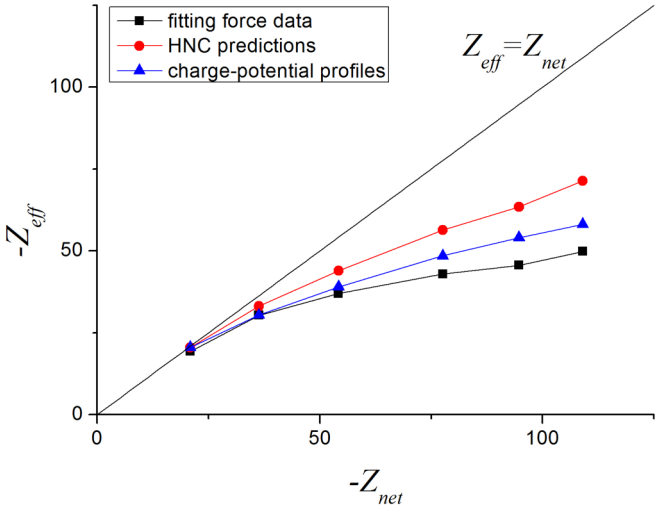

FIG. 7. Effective charges obtained by fitting force data in Fig. 6, predicted by the OZ-HNC theory, and estimated from charge-potential profiles as a function of the net charge.

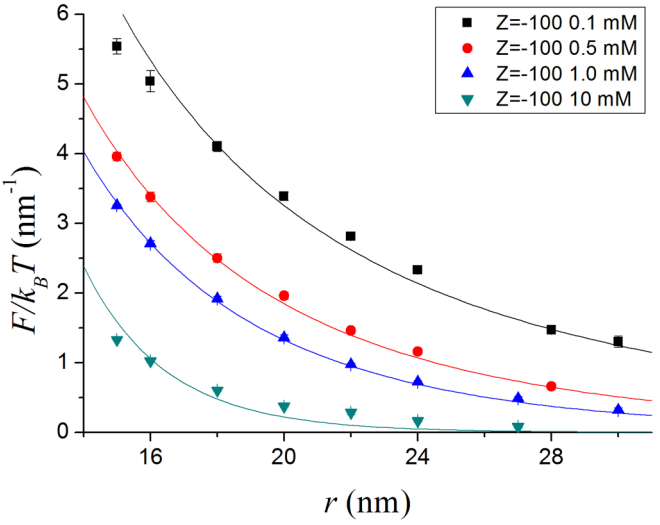

FIG. 8. Force (F) between a pair of nanogels as a function of the distance (r) between their c.m.'s obtained in simulations for the nanogels with $Z = -100$ at different electrolyte concentrations. Lines denote the fits obtained using Denton's potential and the charge as the only adjustable parameter.

Denton some years ago [8], which is similar to the classical Yukawa-like electrostatic interaction potential for hard colloids. In fact, it can be easily proved that Denton's expression exactly leads to the widely known Yukawa [or Derjaguin-Landau-Verwey-Overbeek (DLVO)] form if the bare charge of the nanogel is replaced by the net charge:

$$\frac{U_{nn}^{pmf}(r)}{k_BT} = \lambda_B Z_{\text{net}}^2 \left(\frac{e^{\kappa R_n}}{1+\kappa R_n}\right)^2 \frac{e^{-\kappa r}}{r}. \tag{3}$$

Here λ_B is the so-called Bjerrum length and κ is the reciprocal of the Debye length. Indeed, the expression obtained by Denton can be appealing and friendly for a broad community of scientists and engineers interested in nanogels. Also, a few recent works have estimated the effective charge of nonoverlapping microgels [28,29] assuming this potential; however, it is based on a linear response theory. Consequently, the charge involved must be considered an effective charge rather than a real one. In addition, Denton's potential ignores the fluctuations of charge distributions, the flexibility of polymer chains, and the complex topology of nanogels.

The force derived from such a potential is

$$F(r) = \lambda_B k_B T Z_{\text{eff}}^2 \left(\frac{e^{\kappa R_n}}{1+\kappa R_n}\right)^2 \frac{e^{-\kappa r}}{r^2}(1+\kappa r). \tag{4}$$

Here Z_{eff} is the effective charge (instead of the net charge). In the fits performed in Fig. 6 the only adjustable parameter was the effective charge, whose values are also included in Table I. Analyzing the values of Z and Z_{eff}, it can be easily concluded that the effective charge only increases 64% when the bare charge and the net charge are multiplied by 8 and 3, respectively. In addition, the effective charge considerably deviates from the net charge with increasing the bare charge. In fact, for $Z = -400, Z_{\text{net}}$ is approximately twice larger than Z_{eff}. The discrepancies between Z_{eff} and Z_{net} can be graphically appreciated in Fig. 7, which clearly reveals that: (i) both charges agree only for very low Z_{net} values, and (ii) for larger net charges, Z_{eff} grows much more slowly than Z_{net}. Thus nonlinear effects have outstanding consequences in the nanogels studied here (unlike previous surveys for nanogels with radii greater than 70 nm [9,10]) and an additional procedure for estimating the effective is required. Without such formalism, the capability of prediction of Denton's potential would vanish because the net charge does not characterize electrostatic interactions for highly charged nanogels. Regarding Fig. 7, it should be also mentioned that the effective charge does not seem to reach a saturation value. This behavior is likely to be related to the fact that the nanogel size increases with the net charge.

We have also simulated nanogels with the same bare charge ($Z = -100$) at different electrolyte concentrations ranging from 0.1 to 10 mM. The results are plotted in Fig. 8, which also shows the fits with Z_{eff} as the only adjustable parameter. As can be seen, these data can also be approximately fitted using Eq. (4). It is worth stressing that the effective charges obtained for 0.5, 1, and 10 mM are very similar, although the corresponding net charges differ.

C. Predicting effective charges from charge-potential profiles

A simple and intuitive prescription for predicting the effective charge from the bare charge and electrostatic potential is proposed and explored in this survey. In the case of many nanoparticles simulated here, the electrostatic energy of counterions near the nanogel or inside it is much greater than k_BT (as pointed out previously). Thus some authors say that these counterions are electrostatically bound to (or condensed on) the colloidal particle. There are different criteria to define which counterions can be considered condensed [30]. In this work, however, we have chosen the simplest one: only ions feeling an electrostatic attraction stronger than the thermal energy (k_BT) are bound to the nanogel and contribute to the effective charge. According to the criterion adopted previously, the effective charge corresponds to $|e\psi|/k_BT = 1$ in the charge-potential profiles plotted in Fig. 4.

TABLE II. Values of R and δ describing the charge distribution in the nanogels and employed in the HNC predictions of the effective charge.

$-Z$	Salt concentration (mM)	R (nm)	δ (nm)
25	1	6.14	2.34
50	1	6.42	2.53
100	0.1	6.63	2.49
100	0.5	6.56	2.50
100	1	6.51	2.63
100	10	6.19	2.65
200	1	7.17	2.72
300	1	7.73	2.63
400	1	8.30	2.62

The effective charges obtained in this way are also included in Table I and plotted in Fig. 7 (for 1 mM). As can be seen, these values are close to the effective charge obtained by fitting forces and capture the main features of the qualitative behavior exhibited by Z_{eff}. It is worth stressing that, according to this figure, the systems with $Z = -100$ should have very similar effective charges for 0.5, 1, and 10 mM, although they have different net charges, in agreement with the effective charge obtained by fitting forces in Fig. 8.

D. Predicting effective charges from OZ-HNC

It would be interesting to explore if the quantitative agreement can be improved by employing a more sophisticated scheme. Thus the effective charge was estimated from an OZ integral equation theory for the three-component system formed by nanogels, counterions, and coions, within the HNC approximation. In this theory, the hard-core Coulomb potential was employed for the ion-ion interaction, i.e., $u_{ij}(r) = Z_i Z_j e^2/4\pi\varepsilon_0\varepsilon_r r$ for $r > d$, and $u(r) = \infty$ for $r \leqslant d$ [9]. This theory assumes that the bare charge of the nanogels is uniformly distributed in a core of radius $R - \delta$ and then the charge density decays to 0 in an external shell of thickness 2δ [9]. The values of R and δ (shown in Table II) were calculated from the bare charge density distributions provided by single-nanogel simulations, taking into account that the local concentration of charged monomers decays with the maximum slope at R and vanishes at $R + \delta$, since the local concentration of monomers must vanish beyond their farthest positions. The electrostatic interaction between an ion and the nanogel was computed by integrating the electrostatic field generated by the charge distribution of the nanogel. More details about the explicit expression of the ion-nanogel interaction can be found in Ref. [9].

In the limit of infinite dilution of nanogel particles, the six OZ equations can be split into three subsets. Three of these equations provide the ion-ion pair distribution functions. There are two other equations leading to the ionic density profiles inside and around the nanogel. Finally, the sixth equation makes use of the ion-ion and ion-nanogel pair distribution functions to determine the so-called indirect correlation function between two isolated nanogels immersed in a bulk suspension of ions given by $\gamma_{nn}(r) = g_{nn}(r) - c_{nn}(r) - 1$, where $g_{nn}(r)$ and $c_{nn}(r)$ are the pair distribution function and the direct distribution function, respectively. Although HNC is in fact an approximation that neglects the contribution of the bridge functions to the pair correlation functions, it has two important advantages. First, it leads to realistic predictions for the kind of system and particle interactions addressed in this study by still keeping the simplicity. Second, the HNC allows a straightforward calculation of the effective interaction between microgels. In fact, such effective potential is given by $U_{nn}^{pmf}(r) = u_{nn}(r) + \gamma_{nn}(r)$, where $u_{nn}(r)$ is the bare Coulomb interaction between the charge distribution of both microgels. Once the effective potential has been determined, the corresponding effective charge can be calculated by fitting its asymptotic behavior for large interparticle distances using the following dimensionless form of the Yukawa-like pair potential:

$$\beta U_{nn}^{pmf}(r) = A\frac{e^{-\kappa' r'}}{r'} \tag{5}$$

with

$$A = \frac{\lambda_B}{R_n} Z_{\text{eff}}^2 \left(\frac{e^{\kappa'}}{1+\kappa'}\right)^2, \tag{6}$$

where $\beta = 1/k_B T$, $\kappa' = \kappa R_n$, and $r' = r/R_n$. In order to confirm that the simulation and theoretical results are well represented by this Yukawa potential, the function $y(r') = \ln[r'\beta U_{nn}^{pmf}(r')]$ is plotted. If the nanogel-nanogel effective pair potential has a Yukawa tail, then this function must decrease linearly with r':

$$\ln\left[r'\beta U_{nn}^{pmf}(r')\right] = \ln A - \kappa' r'. \tag{7}$$

The slope of the straight line provides the reciprocal of the Debye screening length κ, whereas the zero intercept obtained by extrapolation leads to the nanogel effective charge. In all cases, the obtained value for κ agrees with the expression $\kappa = \sqrt{8\pi\lambda_B c_s}$, where c_s is the concentration of monovalent salt. In Fig. 9, an example of this fitting procedure is illustrated. The graph displays the function $y(r')$ obtained from the solution of the OZ-HNC equations for $Z = -200$ and a salt concentration of 1 mM. The plot clearly shows the linear decay of $y(r')$.

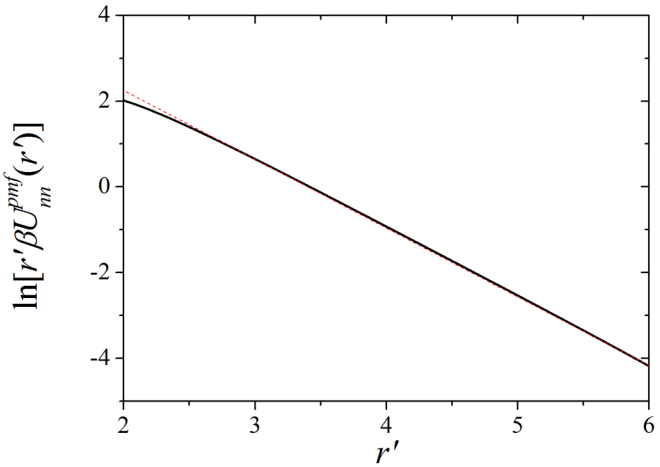

FIG. 9. Function $y(r')$ obtained for the nanogel with $Z = -200$ and 1 mM. The dashed line is the function $\ln A - \kappa' r'$, which illustrates the asymptotic part of $y(r')$.

It should be emphasized that for long interparticle distances, the theoretically predicted effective electrostatic pair potential between nanogels is in all cases very well described by the Yukawa functional form with κ values very close to the theoretical ones. However, the values of the effective charge (included in Table I and Fig. 7) change when the bare charge is modified, exhibiting the same trends as the simulated result: For highly charged nanogels Z_{eff} is significantly smaller than Z_{net} and increases slowly. Thus the predictions provided by the HNC are able to qualitatively capture the behavior reported for Z_{eff}. Quantitatively speaking, such predictions are in general very good for weakly charged nanogels, but they worsen when the nanogel charge increases, as the HNC systematically overestimates the effective charge of the particle, as expected for strongly charged particles.

IV. CONCLUSIONS

Coarse-grained simulations reveal that the electrostatic forces between charged nanogels can be approximately derived from a Yukawa-like potential. This is a nontrivial result because Denton's potential neglects the fluctuations of charge distributions, the flexibility of polymer chains, and the complex topology of nanogels (explicitly considered in the model employed here). In addition, it should be stressed that electrostatic interactions are not always controlled by the net charge of the nanogels. In this respect, two theoretical procedures for predicting the effective charge have been proposed. Both provide predictions of the same order and reproduce to a great extent the behavior reported for the effective charge obtained from simulations.

ACKNOWLEDGMENTS

The authors thank the following institutions for financial support: (i) Ministerio de Economía y Competitividad, Plan Estatal de Investigación Científica y Técnica y de Innovación 2013–2016, Projects No. FIS2016-80087-C2-1-P, No. FIS2016-80087-C2-2-P, and No. FIS2016-81924-REDT and (ii) the European Regional Development Fund (ERDF).

[1] A. V Kabanov and S. V Vinogradov, Angew. Chem. Int. Ed. **48**, 5418 (2009).
[2] J. Ramos, J. Forcada, and R. Hidalgo-alvarez, Chem. Rev. **114**, 367 (2014).
[3] M. Karimi, A. Ghasemi, P. S. Zangabad, R. Rahighi, S. M. M. Basri, H. Mirshekari, M. Amiri, Z. S. Pishabad, A. Aslani, M. Bozorgomid, D. Ghosh, A. Beyzavi, A. Vaseghi, A. R. Aref, L. Haghani, S. Bahrami, and M. R. Hamblin, Chem. Soc. Rev. **45**, 1457 (2016).
[4] P. S. Mohanty and W. Richtering, J. Phys. Chem. B **112**, 14692 (2008).
[5] U. Gasser, B. Sierra-Martin, and A. Fernandez-Nieves, Phys. Rev. E **79**, 051403 (2009).
[6] V. Dahirel and M. Jardat, Curr. Opin. Colloid Interface Sci. **15**, 2 (2010).
[7] C. N. Likos, Phys. Rep. **348**, 267 (2001).
[8] A. R. Denton, Phys. Rev. E. **67**, 011804 (2003).
[9] A. Moncho-Jordá, J. A. Anta, and J. Callejas-Fernández, J. Chem. Phys. **138**, 134902 (2013).
[10] P. Gonzalez-Mozuelos, J. Chem. Phys. **144**, 54902 (2016).
[11] J. Wu, B. Zhou, and Z. Hu, Phys. Rev. Lett. **90**, 048304 (2003).
[12] D. Gottwald, C. N. Likos, G. Kahl, and H. Lowen, Phys. Rev. Lett. **92**, 068301 (2004).
[13] B. J. Riest, P. Mohanty, P. Schurtenberger, and C. N. Likos, Z. Phys. Chem. **226**, 711 (2012).
[14] R. G. Winkler and A. G. Cherstvy, Phys. Rev. Lett. **96**, 066103 (2006).
[15] S. Ulrich, M. Seijo, and S. Stoll, Curr. Opin. Colloid Interface Sci. **11**, 268 (2006).
[16] G. C. Claudio, K. Kremer, and C. Holm, J. Chem. Phys. **131**, 094903 (2009).
[17] P. K. Jha, J. W. Zwanikken, F. A. Detcheverry, J. J. de Pablo, and M. O. de la Cruz, Soft Matter **7**, 5965 (2011).
[18] R. Schroeder, A. A. Rudov, L. A. Lyon, W. Richtering, A. Pich, and I. I. Potemkin, Macromolecules **48**, 5914 (2015).
[19] H. Kobayashi and R. Winkler, Polymers **6**, 1602 (2014).
[20] H. Kobayashi and R. G. Winkler, Sci. Rep. **6**, 19836 (2016).
[21] H. Kobayashi, R. Halver, G. Sutmann, and R. G. Winkler, Polymers **9**, 15 (2017).
[22] N. Gnan, L. Rovigatti, M. Bergman, and E. Zaccarelli, Macromolecules **50**, 8777 (2017).
[23] L. Rovigatti, N. Gnan, and E. Zaccarelli, J. Phys.: Condens. Matter **30**, 044001 (2018).
[24] S. Ahualli, A. Martin-Molina, J. Alberto Maroto-Centeno, and M. Quesada-Perez, Macromolecules **50**, 2229 (2017).
[25] J. N. Israelachvili, *Intermolecular and Surface Forces* (Academic Press, London, 1991).
[26] M. Quesada-Perez and A. Martin-Molina, Soft Matter **9**, 7086 (2013).
[27] M. Quesada-Pérez, S. Ahualli, and A. Martín-Molina, J. Chem. Phys. **141**, 124903 (2014).
[28] P. Holmqvist, P. S. Mohanty, G. Nägele, P. Schurtenberger, and M. Heinen, Phys. Rev. Lett. **109**, 048302 (2012).
[29] M. Braibanti, C. Haro-Perez, M. Quesada-Perez, L. F. Rojas-Ochoa, and V. Trappe, Phys. Rev. E **94**, 032601 (2016).
[30] L. Belloni, Colloids Surf. A **140**, 227 (1998).